Supplementary Information (SI) for ChemComm.
This journal is © The Royal Society of Chemistry 2026

Highly sensitive and Wide-Range Non-Contact Fluorescent Thermometry Based on Well-Defined Cs_2ZrCl_6:Bi Perovskite Nanocrystals

Jinyang Luo[a], Hengjian Mou[a], Jian Wang[a], Chunyu Zhao[a], Chengyu Shi[a], Yanlu Xiong[b,] , Aizhao Pan[a,]**

[a] School of Chemistry, Xi'an Jiaotong University, Xi'an, 710049, China

[b] Department of Thoracic Surgery, Tangdu Hospital, Fourth Military Medical University, Xi'an, China

Corresponding Author

Aizhao Pan

*E-mail: panaizhao2017032@xjtu.edu.cn.

Yanlu Xiong

*E-mail: xiong21@fmmu.edu.cn

Experimental Methods

Material

Caesium carbonate (Cs_2CO_3, 99.0%, AR), Zirconium acetylacetonate ($(C_5H_8O_2)_4 \cdot Zr$, 98%, AR), Bismuth chloride($BiCl_3$, 98.0%, AR), octadecene (ODE, 90%), oleic acid (OA, 90%, AR), oleylamine (OLA, 90%, AR), Acetic acid (99.8%), hydrochloric acid (HCl, 36-38%), Toluene (99.5%), n-hexane (97.0%). All the reagents are directly used without further purification.

Preparation of Cs_2ZrCl_6 and Cs_2ZrCl_6:Bi

In a 50 mL three-necked flask, 10 mL ODE and 0.5 mmol $(C_5H_8O_2)_4 \cdot Zr$ were added. After 2 mL acetic acid was added dropwise to completely dissolve the solid, 0.5 mmol Cs_2CO_3, 2 mL OA, and 2 mL OLA were introduced. The mixture was heated and stirred at 160℃ for 30 min under a N_2 atmosphere, followed by the slow injection of 3 mL hydrochloric acid. After 1 min, the system was cooled in an ice-water bath. The resulting solution was centrifuged at 10,000 rpm for 5 min, and the supernatant was discarded. The precipitate was washed with n-hexane and ethanol three times, respectively, and dried at 60℃ for 24 h to obtain a white powder. Cs_2ZrCl_6:Bi was prepared by dissolving 0.03 mmol $BiCl_3$ in 3 mL hydrochloric acid and injecting it into the above solution.

Temperature response test

A small amount of Cs_2ZrCl_6:Bi powder was spread evenly on a glass slide, which was then placed on a heating stage. The temperature was gradually increased to 160℃, and the emission intensity was measured and recorded at regular temperature intervals.

After holding at 160℃ for 10 min, the heating stage was turned off. During the natural cooling process, the variations in temperature and PL intensity were monitored and recorded. For the thermal stability test, the glass slide coated with Cs_2ZrCl_6:Bi powder was subjected to multiple heating/cooling cycles on the heating stage, and the PL intensity was recorded accordingly.

Time response test

A thin powder layer was rapidly placed onto a glass plate preheated to 100 °C. The real-time variation of photoluminescence intensity was recorded by the instrument at an interval of 50 ms. The response delay caused by the instrument and manual operation (approximately 1 s).

Characterization

TEM and high-resolution TEM (HR-TEM) characterization are collected at 200 kV using a FEI G2F30 electron microscope equipped with Gatan SC 200 CCD camera. SEM and EDS of Cs_2ZrCl_6 and Cs_2ZrCl_6:Bi were observed using a Gemini SEM 500 field emission scanning electron microscope. The powder X-ray diffraction (PXRD) analysis of the obtained sample was carried out by Bruker AXS D8 Discovery X-ray diffractometer at the wavelength of Cu K (1.97 Å). X-ray photoelectron spectroscopy (XPS) was tested by AXIS ULTRA instrument (England, KRATOS ANALYTICAL, Ltd.), which is conducted using the Al mono K α X-ray source (1486.6 eV) at 150 W with the acquisition times of 220 s for chemical element analysis. Ultraviolet and visible absorption (UV-vis) spectra were collected using a Cary 5000 UV-Vis-NIR spectrophotometer. Fluorescence spectra were collected using an integrated sphere on

an Edinburgh Instruments FLS920 spectrophotometer. Fluorescence lifetime is collected through a FLSPP20 steady-state and transient fluorescence spectrometer.

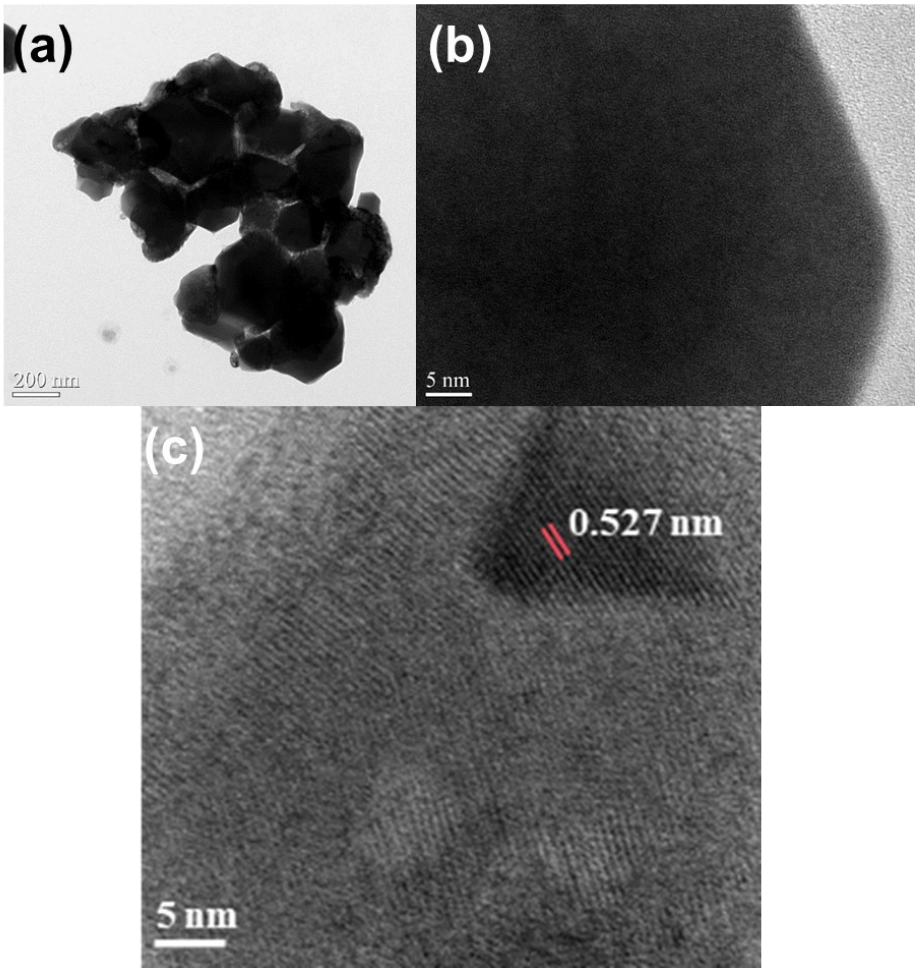

Fig. S1 (a) Additional TEM and (b) HR-TEM images of Cs_2ZrCl_6 and (c) Cs_2ZrCl_6:Bi.

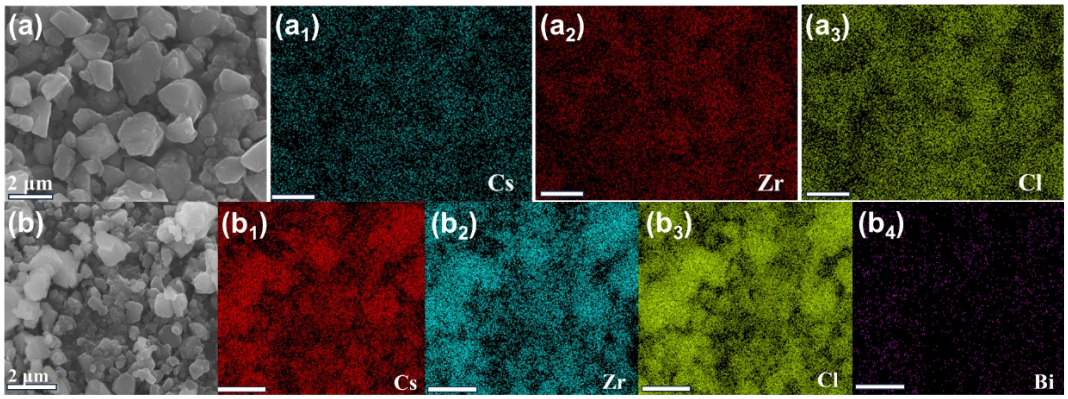

Fig. S2 (a) SEM and elemental mapping images for (a_1−a_3) Cs, Zr and Cl of Cs_2ZrCl_6.

(b) SEM and elemental mapping images for (b_1−b_4) Cs, Zr, Cl and Bi of Cs_2ZrCl_6:Bi.

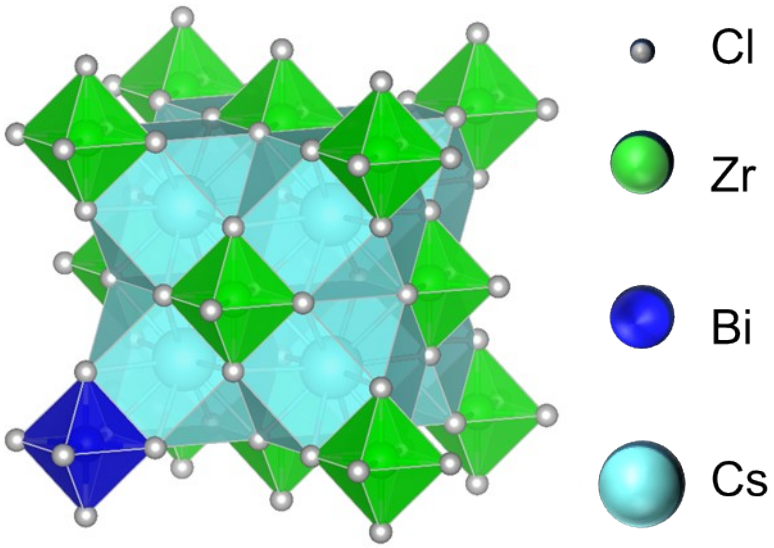

Fig. S3 The crystal structure of Cs_2ZrCl_6:Bi.

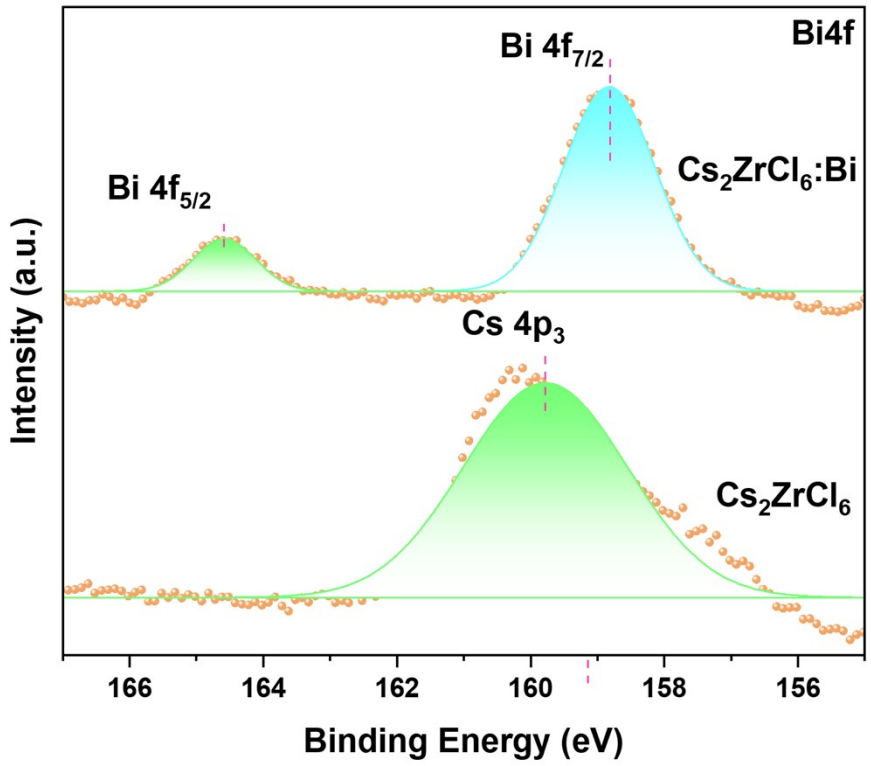

Fig. S4 The high-resolution XPS spectra (167-155 eV) of Cs_2ZrCl_6 before and after Bi^{3+} doping after fitting.

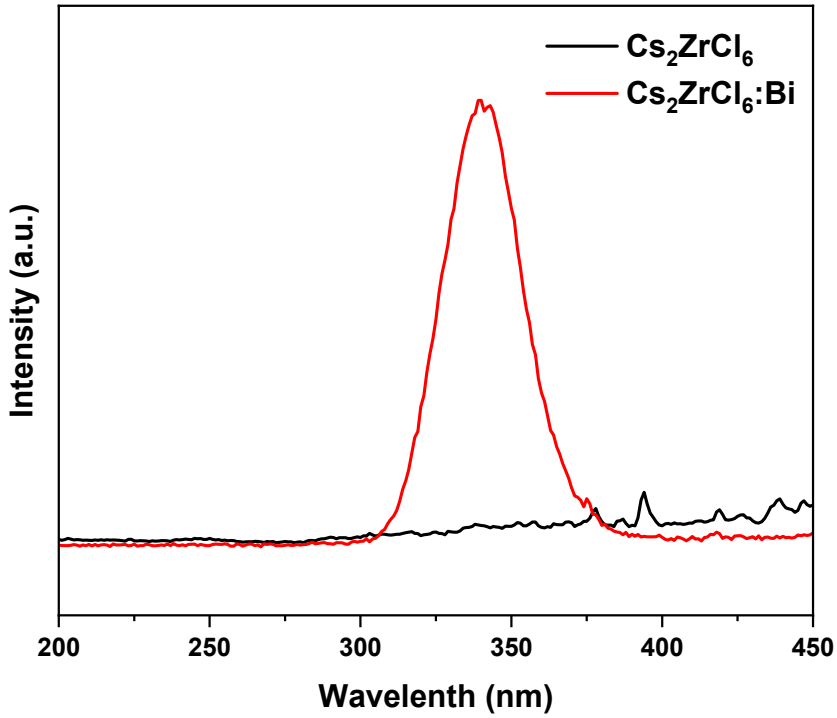

Fig. S5 The excitation spectra Cs_2ZrCl_6 and Cs_2ZrCl_6:Bi.

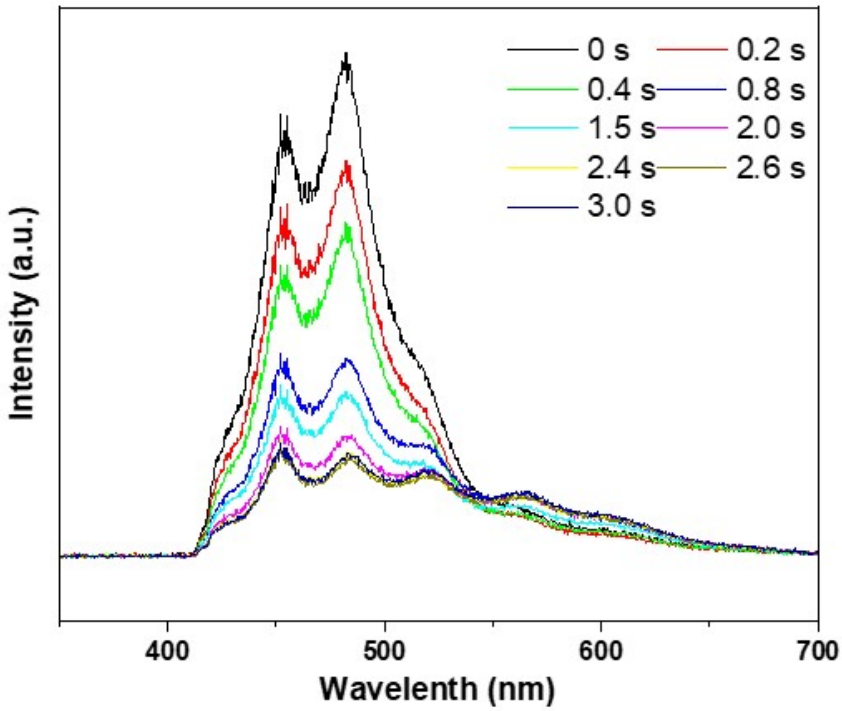

Fig. S6 PL spectra recorded at different time points at 373 K.

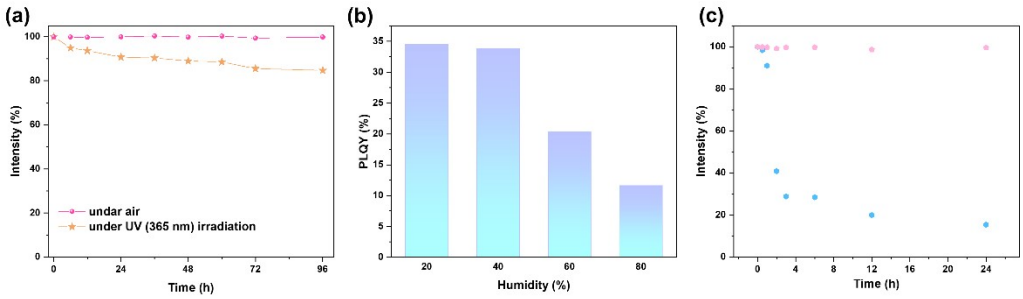

Fig. S7 (a) Cs_2ZrCl_6:Bi under UV (365 nm) irradiation and air over time. (b) Cs_2ZrCl_6:Bi for 24 h under different humidity. (c) Change of PL over time at 20% and 80% humidity.

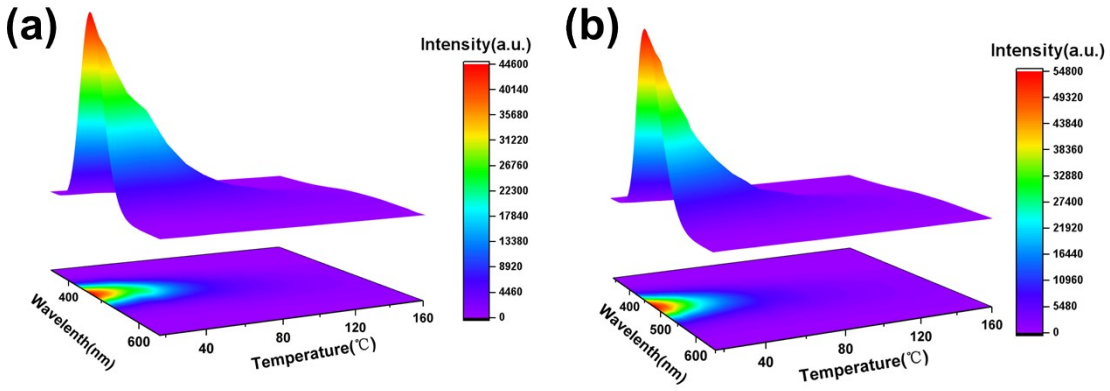

Fig. S8 The supplementary PL mapping spectra of Cs_2ZrCl_6:Bi powder during (a) heating and (b) cooling processes.

Table S1. Fitting curve parameters of PL intensity and temperature for Cs_2ZrCl_6:Bi during heating and cooling processes.

Program	Functional model	A_1	A_2	x_0	dx	R^2
Heating	Boltzmann	102045	997.4	287.46	24.78	0.9965
Cooling	Boltzmann	141050	1887.8	283.69	20.09	0.9987

Table. S2 Comparison of temperature measurements using nanomaterials.

Probe	Temperature range (K)	R^2	S_a (K^{-1})	S_r (%·K^{-1})	Ref.
$CsPbBr_3$@SNF	298-473	0.9951	-	-	1
$CsPbBr_3$/CdTe@SiO_2	298-398	0.9974	0.523 at 298 K	-	2
$CsCu_2I_3$:Eu^{2+}	260-360	0.983	0.091 at 360 K	2.60 at 260 K	3
$Cs_3Cu_2I_5$:Mn^{2+}	298-498	0.9901	0.547 at 498 K	5.25 at 298 K	4
$Sr_4Al_{14}O_{25}$:Eu^{2+}	293-423	-	0.004 at 373 K	0.624 at 373 K	5
$CsPbBr_3$	293-353	0.99	-	1.2	6
$CsPbBr_3$/Cs_4PbBr_6	278-328	0.99	-	1.01 at 278 K	7
$Cs_2AgInCl_6$:Bi and Tb	303-423	0.996	2.15% at 350 K	2.25 at 303 K	8
Cs_2ZrCl_6:Bi	293-433	0.9965	-	1.98 at 293 K	This work

References

1. Y. Chen, X. Chen, C. Zhao, J. Sun, W. Xiong, K. Yan, Y. Zhang, L. He and A. Pan, Chemical Engineering Journal, 2023, 460, 141772.
2. J. Sun, P. Zhang, K. Yan, A. Pan, C. Len, W. Ouyang, C. Shi, X. Shi and J. Hong, Journal of Colloid and Interface Science, 2025, 693, 137607.
3. X. Li, G. Gao, K. Wang, Z. Chen, Z. Gao, Q. Qin, L. Chen and B. Zou, Journal of Rare Earths, 2024, 42, 1429–1436.
4. P. Du, P. Cai, W. Li, L. Luo, Y. Hou and Z. Liu, Microchimica Acta, 2019, 186, 730.
5. M. Wu, D. Deng, F. Ruan, B. Chen, L. Lei, R. Lei and S. Xu, Optical Materials, 2019, 88, 704–710.
6. Z. Lu, Y. Li, W. Qiu, A. L. Rogach and S. Nagl, ACS Applied Materials & Interfaces, 2020, 12, 19805–19812.
7. Z. Lu, Y. Li, Y. Xue, W. Zhou, S. Bayer, I. D. Williams, A. L. Rogach and S. Nagl, ACS Applied Nano Materials, 2022, 5, 5025–5034.
8. R. Song, S. Xu, Y. Li, Q. Zhang, Y. Gao, H. Yu, Y. Cao, X. Li, S. Zhang and B. Chen, Spectrochimica Acta Part A: Molecular and Biomolecular Spectroscopy, 2023, 288, 122181.